Journal of Applied Fluid Mechanics, Vol. 18, No. 3, pp. 769-786, 2025.
Available online at www.jafmonline.net, ISSN 1735-3572, EISSN 1735-3645.
https://doi.org/10.47176/jafm.18.3.2802

Computationally Investigate Low Velocity Hydrokinetic Turbines with Variant Systems

P. P. Gohil[1†], V. Patel[2] and A. U. Mehta[3]

[1] *Sarvajanik College of Engineering & Technology, Surat, Gujarat, 395001, India*
[2] *SardarVallabhbhai National Institute of Technology, Surat, Gujarat, 395007, India*
[3] *Gujarat Technological University, Ahmedabad, Gujarat, 382424, India*

†*Corresponding Author Email:pankaj.gohil@scet.ac.in*

ABSTRACT

A high velocity is rarely accessible in water streams such as rivers, canals, and outlets of sewage and common effluent treatment plants. However, an average velocity of 0.5 - 1.0 m/s is reported to be available in many water streams most of the time. Hydrokinetic (HK) turbines can extract power from the flowing water in these streams. Considering the small quantum of power generated, the economic factor is more significant than efficiency. A Savonius-type HK turbine can generate energy from low-velocity magnitudes of around 0.5 m/s, although it remains a low-speed and low-efficiency turbine. In this study, an attempt has been made to computationally investigate the performance of the Savonius turbine in a water stream channel. It is observed that the performance of the Savonius turbine is not significant, and the generated power cannot be utilized constructively for different applications. Therefore, it is necessary to develop and investigate variant constructive systems to enhance turbine performance. This manuscript focuses on exploring these variant systems and understanding their performance characteristics. Four variant systems have been selected: (i) System-1: Solely Savonius turbine, (ii) System-2: Savonius turbine with a flume, (iii) System-3: Deflector section used before the flume, and (iv) System-4: Deflector section used before the turbine. The investigation was carried out for these four variant systems using the Fluent commercial code. The results indicate that the Coefficient of performance (C_p) is low for System-1, solely Savonius turbine, with a value of 0.052. For the other variants, C_p values were found to be 0.357, 1.385, and 0.579 for the turbine with a flume, deflector before the flume, and deflector before the turbine respectively at the Tip Speed Ratio (TSR) is 1. Moreover, the study also extends to optimizing C_p under different TSR for the different variant systems. The intention is to use this study to install an HK turbine with an optimum constructive structure for maximizing and stabilizing the power that can be used for an isolated application.

Article History

Received May 4, 2024
Revised September 24, 2024
Accepted September 26, 2024
Available online January 1, 2025

Keywords:

Computational method
Low water velocity magnitude
Hydrokinetic turbine
Variant constructive systems
Fluent commercial code

1. INTRODUCTION

Many countries worldwide are increasingly seeking small modular solutions to generate power from independent sources, aiming to reduce dependence on conventional fuels, costs, and emissions. There is a growing preference for renewable sources such as solar, wind, and water, despite various operational challenges. Water, particularly, stands out as a significant renewable energy source. Initial installation costs for hydro turbine units are higher compared to solar photovoltaic (PV) panels, but while PV panel costs rise with unit capacity, hydropower unit costs decrease. Moreover, the capacity factor of micro hydropower units exceeds that of solar PV units. According to the IRENA Renewable Cost Database 2019, the levelized cost of energy (LCOE) for solar PV plants averages around 0.069 USD/kWh, whereas small hydropower projects achieve a lower weighted-average LCOE of 0.041 USD/kWh (Riglin et al., 2015). Hydroelectric power also offers higher energy concentration than wind or solar power (Ponta & Dutt, 2000). However, large-scale hydroelectric systems face challenges such as displacement of communities, land mitigation issues, and high construction costs, leading to significant environmental impacts (Ponta & Dutt, 2000; T. Asim et al., 2013; Wahyudi et al., 2013; Driss et al., 2013).

Table 1 Summary of the published work

Sr. No.	Turbine	Methodology	TSR	Fluid Flow Velocity (m/s)	Max. C_P	Max. C_T	References
1	Savonius Turbine	CFD	0.4,0.8,1.2	0.48	0.29	--	(Alizadeh et al., 2020)
2		CFD	0.5-1	0.2-1.6	0.5	--	(Thakur et al., 2019)
3		CFD	0.8-1.2	--	0.24	0.27	(Kerikous & Thévenin 2019)
4		Experiment CFD	0.2-1	0.86	0.12	0.25	(Mosbahi et al., 2019a)
5		Experiment	0.4-2	0.56	0.5	0.55	(Patel et al., 2019)
6		Experiment	0.3-1.5	0.8	0.29	0.41	(Talukdar et al., 2018)
7		CFD	0.6-1.8	--	0.27	0.37	(Elbatran et al., 2017)
8		CFD	0.5-1	0.5-2	0.38	--	(Kumar et al., 2017a)
9		CFD	0.5-1	0.5-3	0.426	--	(Kumar et al., 2017b)
10		Experiment	0.5	0.46	0.2	0.5	(Patel et al., 2017)
11		Experiment	1.1	0.8	0.25	--	(Nakajima et al., 2008)
12		Experiment	0.82	0.45	0.21	0.26	(Golecha et al., 2011)
13		Experiment	1.1	0.45	0.35	0.32	(Golecha et al., 2012)
14		Experiment CFD	0.77	0.3-0.9	0.39	--	(Sarma et al., 2014)

Consequently, current research and technology are focusing on supporting small-scale hydro power systems, which are considered among the most cost-effective and environmentally friendly technologies for rural electrification.

The utilization of hydrokinetic energy systems, which harness the power of flowing water in open channels, holds significant potential for meeting local electricity demands. This approach offers several advantages, including reduced reliance on extensive regulatory measures and substantial capital investments typically combined with conventional water impoundment methods. Furthermore, due to its high energy density, dependability, and low environmental impact, this technology is becoming increasingly appealing among renewable energy sources (Roy & Saha, 2013; Zhou & Rempfer, 2013; Mohamed et al., 2015). Many rural communities and farms are located near rivers with little or no elevation, making it difficult to employ traditional micro-hydro generation in such situations (Mohamed, 2012; Johnson & Pride, 2010). This highlights the potential advantage of hydrokinetic technology, which may offer more viable sites compared to traditional hydropower generation (Kusakana & Vermaak, 2013; Mohamed, 2013).

There is a need to gain a deeper understanding of the possibilities for hydrokinetic (HK) energy development in established canal systems that are already equipped with integrated hydropower plants. Exploring these opportunities can provide valuable insights into maximizing the utilization of these existing infrastructure assets for harnessing HK energy. Among many of the HK turbines, Savonius turbine works on the drag force produced by the blades. It has high starting torque with low speed and is economically very sound. However, its efficiency is low. On the other side Darrieus type is an efficient turbine; but requires high-velocity flow and is not self-starting. A positive aspect of the Savonius turbines is that it can extract power even from very low velocity, making it suitable for low power isolated applications like pumping water for irrigation purpose, night light vision and others. Additionally, inconsistent flow of water during different seasons in canal or rivers is a confounding factor in this regard.

Canals, in their existing forms, exhibit diverse courses and volumes designed to fulfill their primary functions of facilitating irrigation, navigation, and hydropower generation. Canals specifically intended for navigation purposes typically feature low velocities, often falling below the minimum speed required for turbine activation. Consequently, these canals generally offer limited potential for the development of hydrokinetic energy systems. Favourable characteristics for economically viable HK energy development can include high current speeds (>1.5 m/s) corresponding to good site access (Mohamed et al., 2010). However, such velocity is not available in the canal and river throughout the year. The average velocity available in such water streams could be around of 0.5 m/s with a range of 0.5 -1.0 m/s during most part of the year. Such velocity range is favourable for installation of the Savonius turbine as reported earlier (Castelli et al., 2011; Mohamed et al., 2011; Mohamed et al., 2011). Much research has been done on specified hydrokinetic turbines, however most studies investigated on higher water current or velocity, with few studies using just numerical models (Kumar & Saini, 2017a, b). Table 1 depicts a summary based on work done by researchers to improve the performance of the zero head turbine unit using experimental and numerical approaches. The Coefficient of performance (C_P) & Coefficient of torque (C_T) are presented using Eq. (1) and Eq. (2) respectively.

$$\mathbf{C_P} = \frac{\mathbf{P_0}}{\mathbf{P_{th}}} = \frac{\frac{\mathbf{2\pi NT}}{\mathbf{60}}}{\frac{\mathbf{1}}{\mathbf{2}}\boldsymbol{\rho} \mathbf{A V^3}} \tag{1}$$

$$C_T = \frac{4T}{\rho V^2 D^2 H} \tag{2}$$

where, ρ is the water density (kg/m^3), V is the flowing velocity of water (m/s), A is the turbine frontal area (m^2), D is the turbine rotor diameter (m), H is the rotor height (m), N is the rotational speed (rpm), and T is torque(Nm).

Furthermore, researchers have explored arranging hydrokinetic turbines in various arrays to enhance power generation (Nag & Sarkar, 2021; Chen et al., 2022). However, increasing the number of turbines raises costs

Fig. 1 Satellite picture utilized from Google map for selection of a site

and maintenance requirements, while also introducing operational complexities. In open channels, the velocity profile varies along the channel height, with maximum velocity typically occurring near the top. In contrast, closed channels exhibit maximum velocity at the center, potentially resulting in a more uniform velocity profile across the turbine shaft and thereby promoting uniform torque generation. However, closed channels are disadvantaged by extended wake formation. Therefore, it is crucial to conduct studies to investigate closed structures, aiming to achieve uniform velocity distribution across the shaft and to understand the formation and impact of wakes at different distances.

The initial stage in designing and building a hydrokinetic turbine involves determining the size of the turbine rotor. This process commences by estimating the power demand and gaining insight into the average velocity of the local water current. To fulfill the energy requirements for remote areas, there is a need to develop an appropriate, locally fabricated, cost effective and low maintenance system. Many studies have focused on optimizing the runner blade profile for efficiency, these designs frequently encounter fabrication difficulties, especially when trying to maintain complex design parameters. In this study, it is intended to address this by selecting an optimized profile that is not only efficient under low velocity conditions but also simpler to fabricate. Furthermore, we emphasize improving supplementary systems that enhance overall system efficiency, considering the fabrication constraints. With this adaptability, four systems were selected for investigation: (i) System-1: This system solely utilizes the optimally selected Savonius turbine, (ii) System-2: After conducting numerous simulations, a flume was developed to optimize water flow. Based on pressure and velocity contours and vector results, this system ensures smooth water flow through the channel with minimal turbulence, (iii) System-3: To accommodate a higher water flow using the deflector before the flume, the upper and lower spaces were opened in this system, and (iv) System-4: This system incorporates a deflector before the turbine to optimally pass the water over the runner blade.

This study provides an overview of field test carried out for assessment of the available water velocity with due respect to select the optimum Savonius HK turbine and; based on its performance, to develop the different variant systems and investigate the performance parameters of the all variant systems. This study follows the problem formulation for any site in consideration of all site selection parameters and then carrying out measurements as per IEC 60041/IS 41 (1991). Based on the potential of velocity, the turbine is selected and investigated by numerical method. In order to find its results, the other three optimal variant systems are developed and investigated. Finally, the results are analysed and discussed for performance parameters, i.e. pressure, velocity, torque and coefficient of performance of all different systems.

2. PROBLEM FORMULATION

The study site under consideration is located in the Tapi basin in the western part of India. A pre-feasibility site investigation was conducted to assess various cross-sections, including water velocity, location accessibility, the feasibility of installing the unit, and potential power production. Initially a few points were identified and considered based on the satellite image as illustrated in Fig. 1(Google map web). In the next stage, the site visit

Fig. 2 Picture of the final point selected for the velocity measurement

Fig. 3 Photographs of field test of velocity measurement

was completed and based on the possible access, a point was finalized for measurement of velocity (Fig. 2).

In order to measure the velocity of water in the selected canal, a field test was performed to ensure availability of water in the canal. On consultation with the relevant authorities, the water available in the canal at the time of this investigation was found to be average of that available throughout the year. During the peak supply, the water flow was observed to be approximately 25% higher than this average. Locations for velocity measurements were selected based on guidelines from IEC 60041/IS 41 (1991), considering the dimensions of the canal.In-Situ Condition

The Propeller Current Meter (PCM) used here (Make: The National Instrumentation Corporation, Roorkee) had an operating range of 0.1 - 3.5 m/s with an accuracy of >0.3 m/s; 0.5 % full scale. In order to hold the current meter as per specified location, a customized structure was developed. On field, the team successfully placed the mounting structure for measuring the velocity at the specific point as per IEC 60041/IS 41. 1991 at the site specified (see Fig. 3). The reading was recorded in the data logger for 30 sec time period as against IEC 60041/IS 41. 1991, of 20 sec duration, and repeated twice.

The compiled values of measured velocity at all allocated points displayed in the drawing of the canal (Fig. 4) were used for calculating the discharge.

Figure 4 illustrates the measured potential velocity within a specified area measuring 6.5 m in length and 1.8 m in depth (box highlighted in black color). Using this data, velocity profile curves were generated at five key locations, representing significant velocity magnitudes, treated as planes or sections: X0 at the center, X1 at 1.625 m to the right of center, X2 at 3.25 m to the right of center, X1' at 1.625 m to the left of center, and X2' at 3.25 m to the left of center (see Fig. 5).

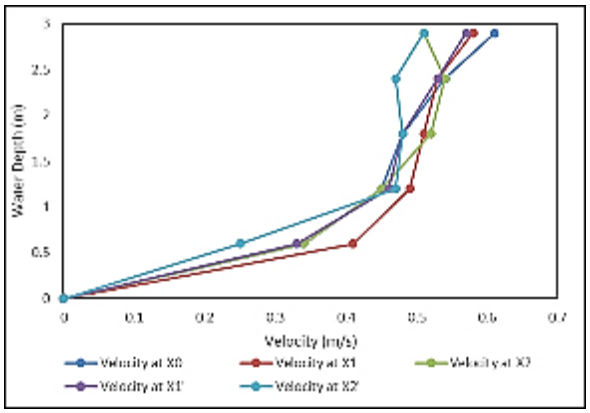

Fig. 5 Velocity profile against depth at five different locations

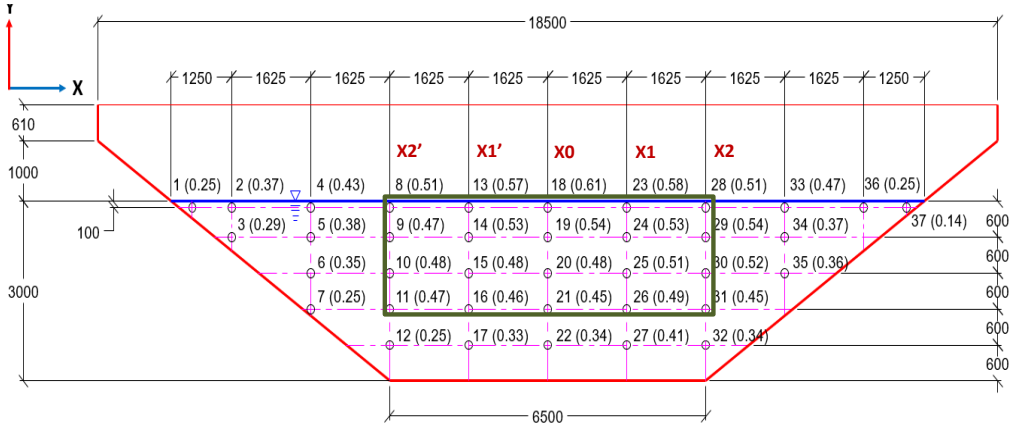

Fig. 4 Velocity magnitude at respective allocated point

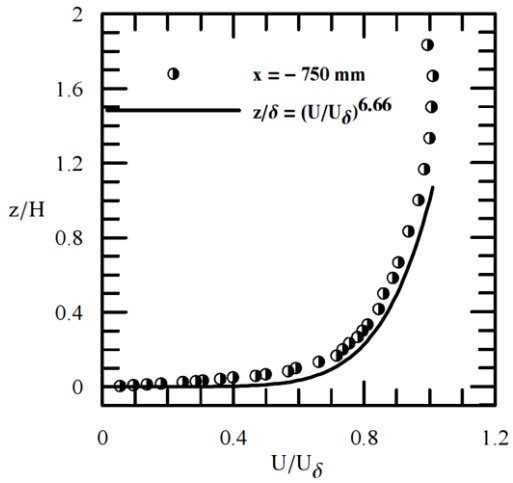

Fig. 6 Velocity profile reported earlier (Loureiro & Silva Freire, 2005)

Figure 5 clearly shows that the water velocity within a channel is not uniform throughout its depth. It gradually increases from zero at the bottom of the channel (invert) to its maximum value near the surface, following a logarithmic distribution pattern similar to that found in open channels (see Fig. 6). The maximum velocity, 0.61 m/s, was observed at the water surface, with an average canal velocity of 0.51 m/s. This potential velocity is available in the canal year-round. During peak conditions, the velocity increases by approximately 25%, reaching 0.64 m/s. As previously mentioned, a velocity of more than 0.5 m/s is often required for hydrokinetic turbines. An uncertainty study on the measurement of liquid flow in open channels using the velocity area method, as per ISO 748: 1997(E), is provided in Appendix I.

To ensure the high-efficiency functioning of a hydrokinetic (HK) turbine, and based on the in situ testing conditions data, it is necessary to understand the optimal Savonius-type HK turbine (details of the drawing is provided in Appendix II) and to study its various parameters and performance.

Simulation results for System-1, along with previous studies, clearly demonstrate that a Savonius turbine alone cannot generate sufficient power for practical applications. Therefore, an augmentation arrangement with the Savonius turbine is required. It is also necessary to investigate all developed augmentation arrangements. The four stages of development, considered as different systems, are depicted below:

3. METHODOLOGY

In this section, System-1 is explained in detail corresponding to the modelling, meshing, pre-simulation and post simulation. Initially, SOLIDWORKS 2022 student edition was used to create a geometrical model of a three-dimensional Savonius hydrokinetic turbine in an open test channel. For performing the numerical analysis, entire domain was submerged into open test channel as shown in Fig. 7. This domain was then divided in two zones i.e., stationary zone (i.e., channel) and rotating zone (i.e., rotor). To construct the rotating zone, a cylindrical volume containing the Savonius HK was built around its vertical axis to allow the turbine to revolve at a given angular velocity during numerical analysis. To guarantee that the flow field remains uninterrupted, the circumference of the cylindrical volume was specified as an interface.

Table 2 Optimum Mesh Parameters of the System-1

Parameters	Stationary zone	Rotating zone
No. of Elements	3462283	1642097
Skewness (avg.)	0.79	0.85
Aspect ratio (avg.)	10	10
Orthogonal quality (avg.)	0.99	0.99

The ANSYS meshing interface is employed in this study to generate the mesh for the entire computational domain. Each sub-domain is meshed using a non-conformal unstructured grid comprising tetrahedral elements, illustrated in Fig. 8 for System-1. Particularly in the rotating section, a finer grid is implemented compared to the stationary zone. A mesh independence study (see Fig. 9) is conducted on System-1, varying mesh sizes and parameters across four configurations to determine the optimal mesh structure (details provided in Table 2). The final mesh is selected based on cells with quality greater than 0.6, skewness greater than 0.83, and aspect ratios less than 12.

The quality mesh parameters were evaluated across all systems. The completed mesh geometry was imported into the Fluent commercial code for the pre-simulation process, where input boundary data under appropriate conditions were applied. Figure 7 depicts the computing domains of the model along with its boundary conditions. The diagram illustrates that the free stream velocity flows from the left side of the channel, corresponding to the inlet velocity, towards the outlet on the right. The outlet of the channel is configured as a pressure outlet, with atmospheric pressure as its reference value. The side and bottom faces of the domain are designated as walls with free-slip boundaries, while the top of the channel is designated as a symmetry surface. The Savonius turbine, located within the rotating zone, is assigned a rotating wall condition (no-slip wall). Similar methodologies and turbulence models have been adopted in several studies (Sarma et al. 2014; Kolekar & Banerjee, 2015; Kumar & Saini, 2017a, b). The selection of the turbulence model and its mathematical expression are presented in Appendix III.

In addition, the rotating zone is subjected to Multiple Reference Frames (MRF), where equations are solved in a rotational reference frame. Consequently, the rotating zone is established by providing a rotational velocity in the absolute reference frame. The Savonius rotor's wall boundary condition then has zero relative speed with respect to adjacent cells. The details of the input parameters selected for the simulation are provided in Table 3.

(i) System-1: Solely Savonius turbine

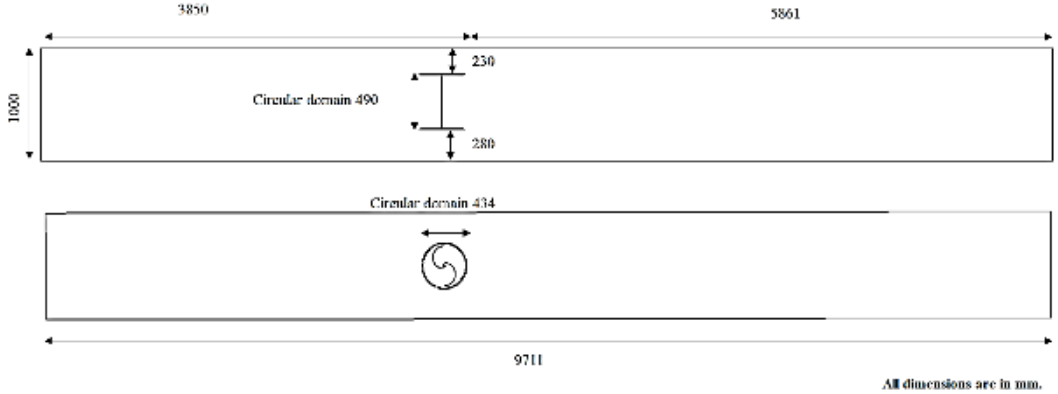

All dimensions are in mm.

(ii) System -2: Savonius turbine is installed with a flume

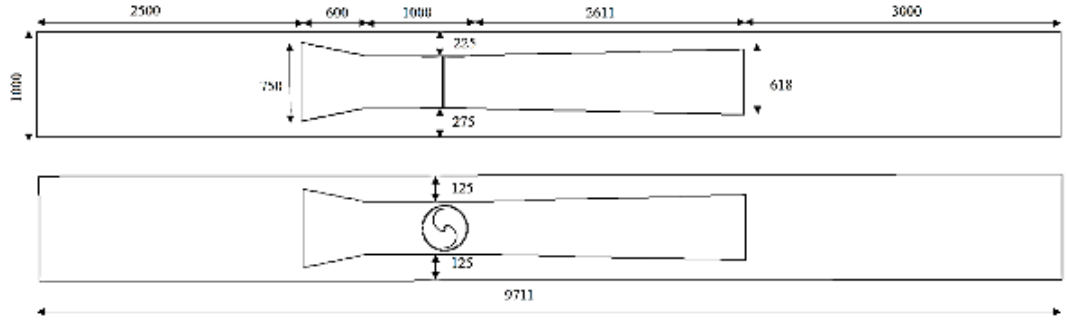

All dimensions are in mm.

(iii) System-3: Deflector section of the flume

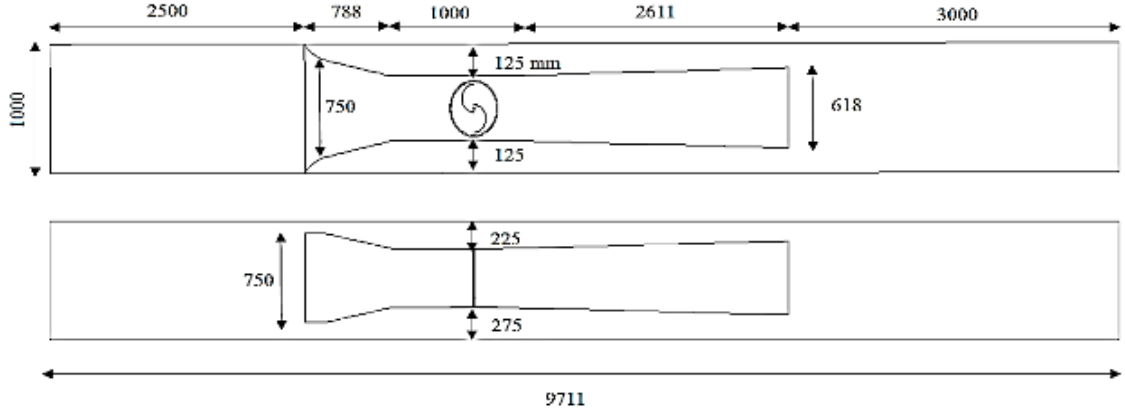

All dimensions are in mm.

(iv) System -4: Deflector section used before the turbine

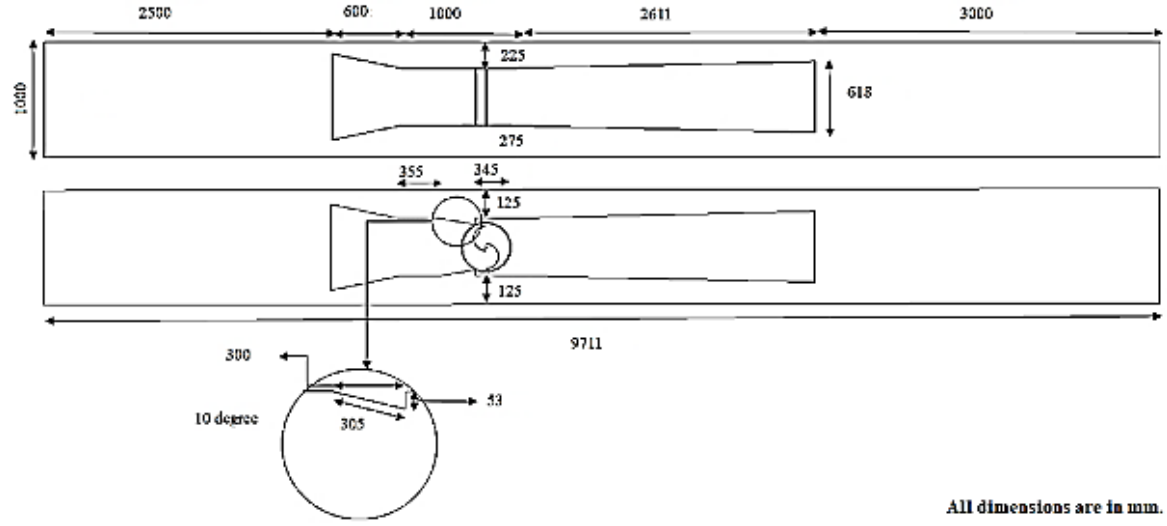

All dimensions are in mm.

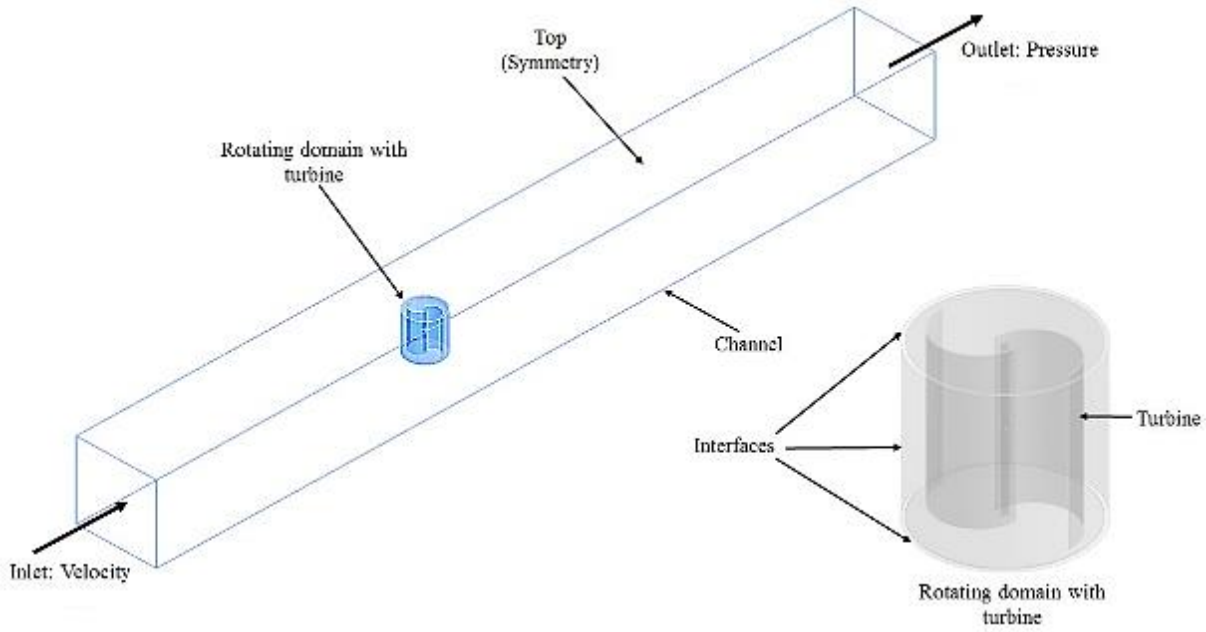

Fig. 7 Computation domain of Savonius turbine with its boundary condition

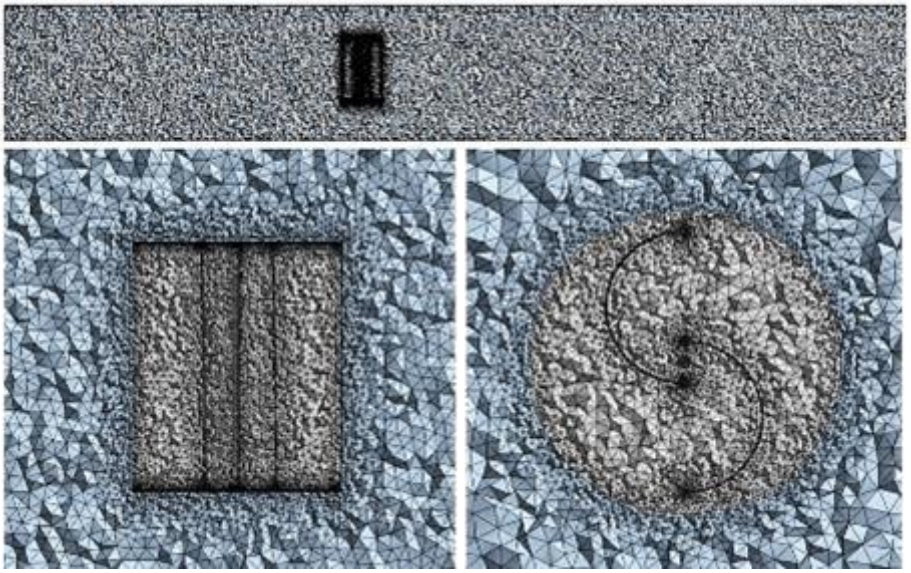

Fig. 8 Meshing view of channel along with dense mesh in rotating zone for the System-1

Table 3 Details of input parameters considered for the simulation

Sr.No.	Parameters	Description considered
1	Components	Stationary domain-I: Test Channel
		Stationary domain-II: Fume, and Deflector
		Rotating domain: Rotor
2	Grid Type	Unstructured mesh (Triangle, Tetrahedron, Hexahedron and Quadrilateral)
3	Analysis type	Steady state
4	Fluid	Water at 25°C
5	Boundary Condition	Inlet: Velocity (Applying Power law equation, using max. velocity of 0.61 m/s)
		Outlet: Static pressure: 1 atm
		Reference pressure: 0 Pa
		Test Channel: Top surface symmetry
		Turbine: Moving wall
6	Turbulence Model	realizable k-ε
7	Convergence Criteria:	RMS < 10E-5

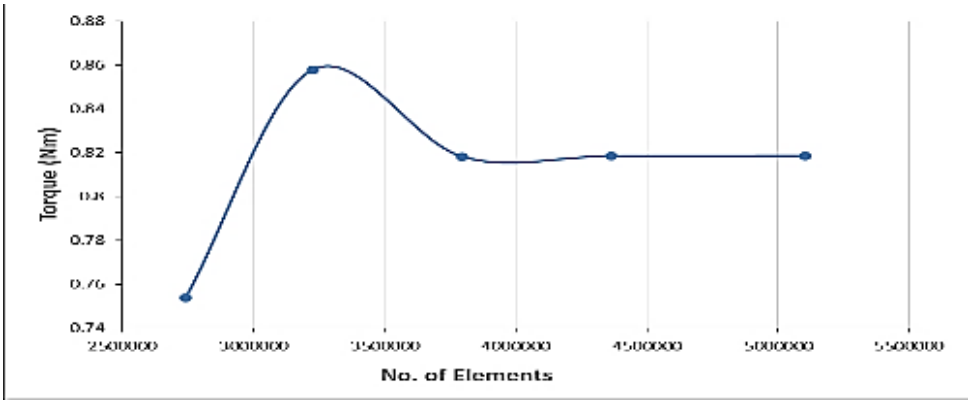

Fig. 9: Grid independency test

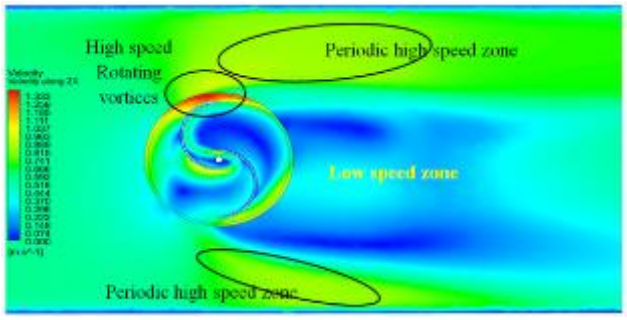

Fig. 10 Velocity contour under the present study for System- 1

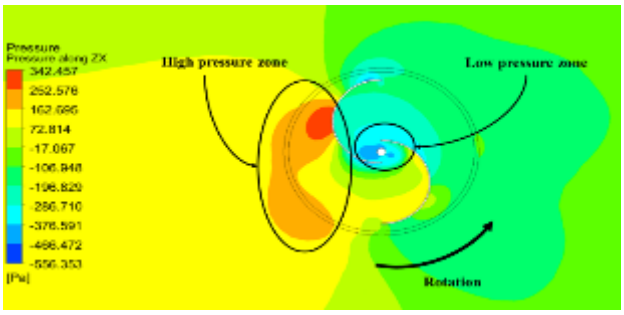

Fig. 11 Pressure contour for System -1 under the present study

After performing the simulation, it was ensured that the converging parameters were solved steadily. The torque value was monitored at the axis of the rotor shaft. The same methodology and parameters were applied to the other three systems. Based on the observed simulation results, the pressure, velocity, coefficient of torque, and power parameters are presented and discussed

4. VALIDATION OF THE SIMULATION RESULT

To validate the performance of the Savonius turbine, simulation results were compared with those of identical turbines operating under similar conditions (Kumar & Saini, 2017a; Zhang et al., 2017). Based on the obtained results, the velocity contours in different regions around the blade were analyzed. Figure 10 shows the velocity pattern at the inlet, which was consistent with the given boundary conditions. The rotation of the turbine leads to the formation of distinct velocity zones. A high-speed zone is observed at the tip of the blade, while a low-speed wake zone forms behind the rotor blades due to the turbine's rotation. This wake zone causes significant reductions in flow velocity in the surrounding area. However, periodic increases in flow velocity occur on the upper and lower sides of the wake zone, forming what is known as the "periodic high-speed zone." This phenomenon results in periodic fluctuations in the velocity pattern, characterized by alternating areas of reduced and heightened flow velocity.

A drop in the pressure contour was detected across the rotor from the upstream to the downstream side. Pressure is uniform at the channel's inlet, and higher pressure values are seen on the inlet side, i.e., the concave side of the advancing blade and the convex side of the returning blade. On the downstream side, a lower pressure area develops (the convex side of the advancing blade). As a result, two pressure areas, higher and lower, are observed near the blades within the flow domain, resulting in a pressure drop. This pressure drop across the rotor causes the turbine blades to initiate revolving, resulting in power extraction from the flowing water in the channel by the Savonius hydrokinetic turbine. In Fig. 11, the pressure contours obtained for a System -1. It is clearly seen that under present study, the pressure distribution patterns observed across the turbine rotor which is in good agreement with many studies (Zhao et al., 2009; Roy & Saha, 2013; Wahyudi et al., 2013; Shashikumar et al. 2021a, b; Singh & Kumar, 2022).

This finding supports the consistency and reliability of the reported results in relation to earlier research. It can see from the figure, it becomes apparent that the pressure reaches its maximum value on the upstream side of the flow near the blade's surface. Conversely, a lower pressure zone is observed on the downstream side of the flow. The disparity between these two pressure zones drives the rotation of the blade.

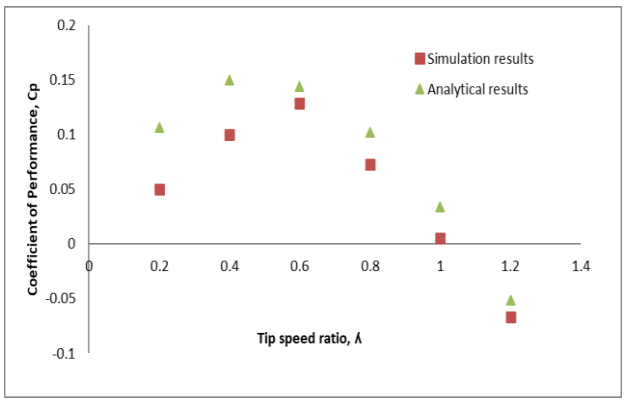

Fig. 12 comparison of results obtained from the present study and analytical model

To verify the computational model quantitatively, the obtained simulation results were compared with the standard analytical model discussed by Patel et al. (2018). This comparison included the results for the coefficient of performance (Cp) and tip speed ratio (λ) from both the simulation and analytical models (see Fig. 12). As seen in the figure, the present study yields a comparable curve. The maximum Cp of 0.129 was obtained at a λ of 0.6 in the present study, which slightly differed from the analytical study where the maximum Cp of 0.15 was obtained at a λ of 0.4. The maximum variation in magnitude was observed at low λ values (0.2 and 0.4), while the minimum variation in magnitude was found for λ values between 0.6 and 1.2.

5. RESULTS AND DISCUSSION

After quantitative and qualitative validation, ensuring the computational results are in close agreement with previous studies, the same methodology was applied to the other three systems. The results of the computational process for all four systems (System-1, System-2, System-3, and System-4) are analyzed in this section. The pressure and velocity distributions are displayed in contour form, along with their performance characteristics, including the coefficient of torque and power.

5.1 Velocity Contours

Figures 15 and 16 depict the velocity variations near the turbine blades in the longitudinal plane (i.e., at the mid-plane) using vectors and contour plots, respectively. The vectors provide insight into the direction of water flow. Analysis of wake generation over the turbine rotor reveals vortices visualized both ahead of the advancing blades and behind the returning blades across all four cases. In System-1, more reverse vectors (illustrated by the curve in Fig. 13) are predicted near the blades, diminishing along the channel distance.

In other systems, the low or weak intense vectors leading to vortex or wake vortices are predicted near the blades. However these low vectors are present throughout the long distance of the channel. Comparing all systems, System-3 experienced low vortices near the blade. It was not exactly in front of the advancing blade. It was present at the trailing edge of the blade. In the System-4, an area with high-intensity vectors exhibiting significant magnitude was identified as a deflector zone. This particular vector pattern suggests a reduced level of momentum exchange between the water stream and the turbine rotor. The study conducted by Sarma et al. (2014) similarly highlighted a decline in performance attributed to sharp velocity vectors. The velocity along the upstream side of the rotor is limited by the applying same inlet boundary conditions.

As clearly seen from the Fig. 16, the velocity range was observed in the range 0-1.379 m/s across the mid-plane of the channel section for the System -1 while the water is flowing smoothly in the channel. The low velocity zone or rope predicted was about 1 -2dr (i.e., d_r is the diameter of the turbine rotor). As for the velocity range in the same mid-plane contour, it was found to be 0-2.332 m/s, 0-3.355 m/s, and 0-2.407 m/s for System-2, System-3, and System-4, respectively. The low velocity zone or rope was found to be 1-10d_r, 1-8d_r, 1-12d_r for the system-2, 3 and 4 respectively. Evidently, in the System-1, the low velocity rope was short as compared to the other systems. However, performance of just the turbine is not significant. On comparing the other systems, System-3 had the lowest velocity rope length than System-2 and 4. The velocity of the flow decreases as it approaches the ducted area; however, the velocity increases as it passes through the converging region. This is less evident in System-3, as velocity remains almost uniform at the enhanced region and improves as it reaches the rotating domain. Within the rotating zone, velocity remains weak on the convex side of the returning blade. All the observations show that vortices occur on the concave surface of both the advancing and returning blades. As a result of the drag force, a high-velocity zone emerges at the attack point of the advancing and returning blades. This drag force is increased for System-3 and is assigned the highest value. Furthermore, a very weak velocity zone is displayed across the concave side of the returning blade downstream of the rotor. This divergence is caused by the centrifugal force induced by the counter-clockwise rotation of the turbines and serves as an indicator of the wake phenomena. This wake zone propagates up to the augmented portion, where velocity increases as it moves away from the rotor. Comparing systems, System-3 displays higher velocity magnitudes and consequently anticipates higher torque.

5.2 Pressure Contours

As discussed in the validation section, the pressure differential across the rotor facilitates blade rotation, enabling the turbine to generate power from flowing water. Figure 15 depicts the pressure contour for all four examples along the ZX plane, with a velocity of 0.588 m/s at a tip speed ratio (TSR) of 1. This diagram clearly illustrates uniform pressure along the rotor's upstream side, indicating a high-pressure zone. Conversely, pressure decreases, forming a low-pressure zone on the downstream side. In all scenarios examined, a depression zone is created behind the advancing blade and on the concave side of the returning blade. In all cases, the pressure on the convex side of the returning blade is significantly higher than that on the concave side of the

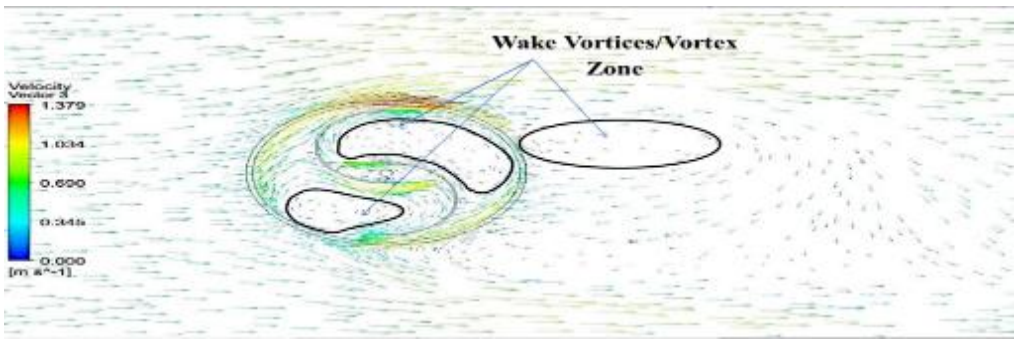

System-1

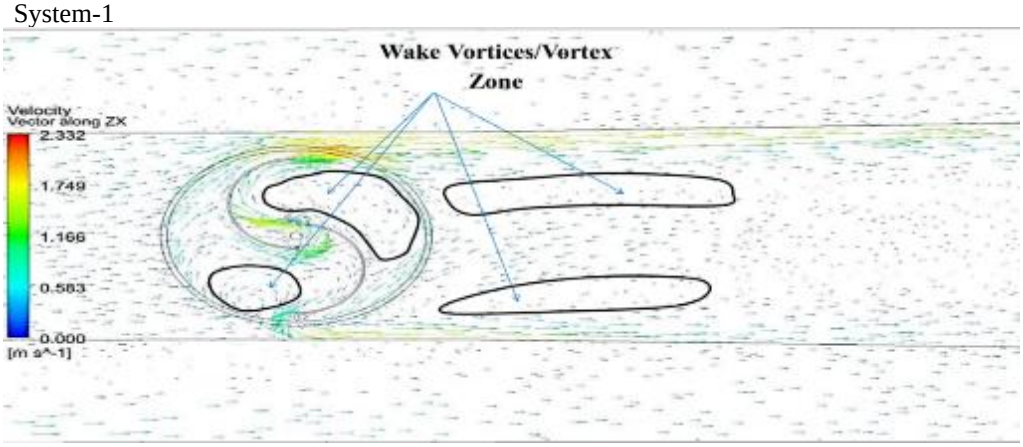

System-2

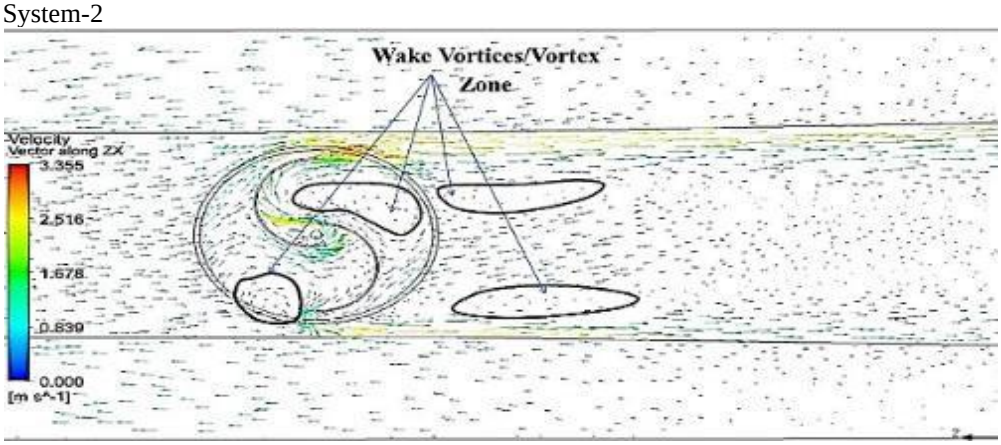

System-3

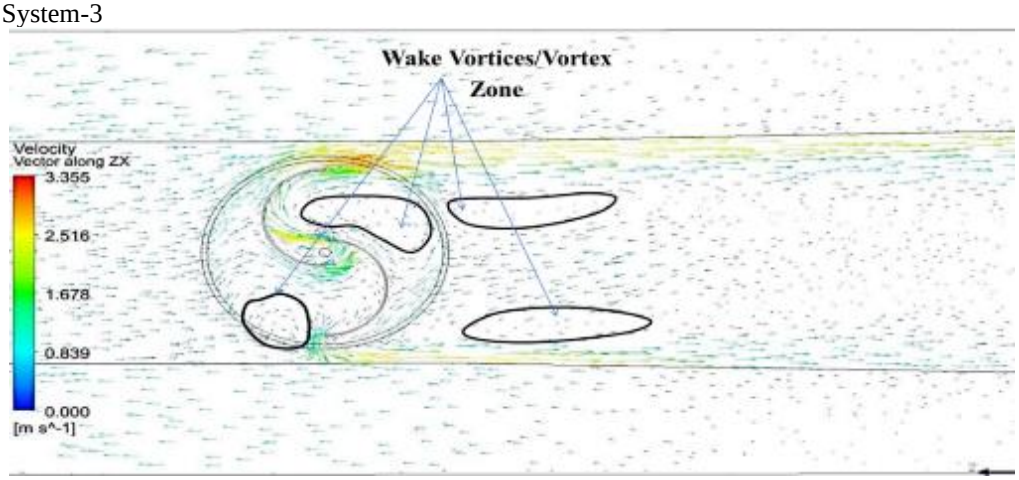

System-4

Fig. 13 Velocity vectors of all cases at TSR = 1

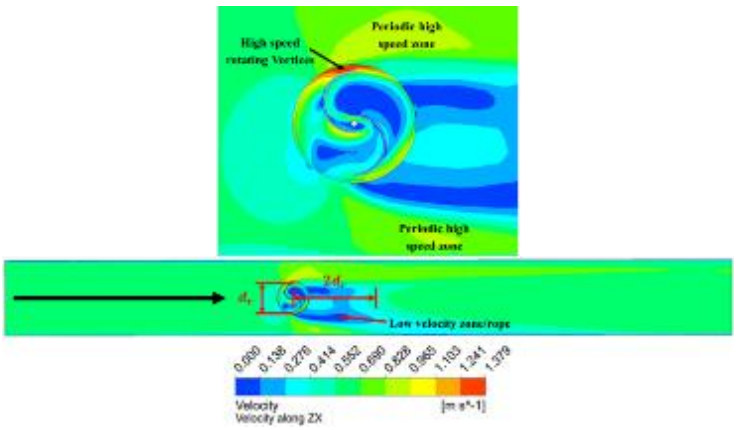

(a)System-1

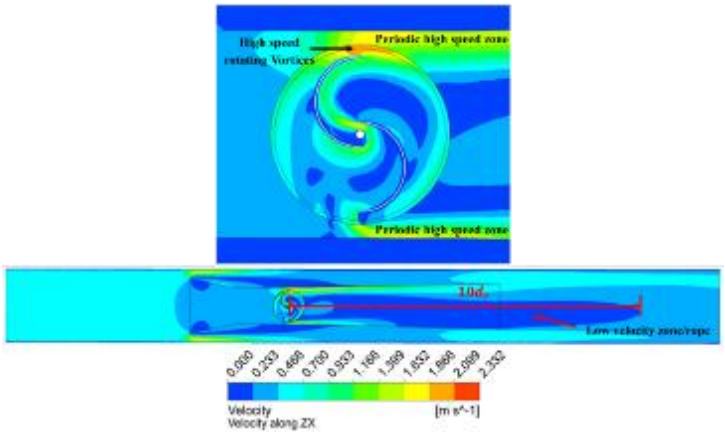

(b) System-2

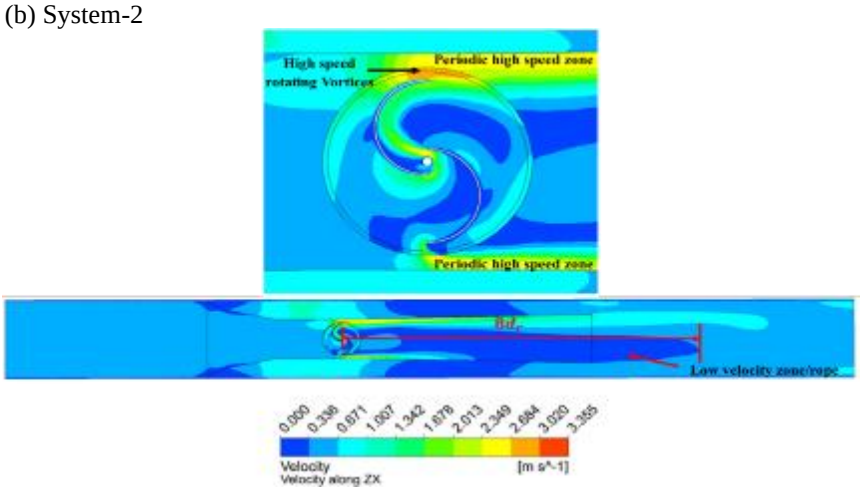

(c) System-3

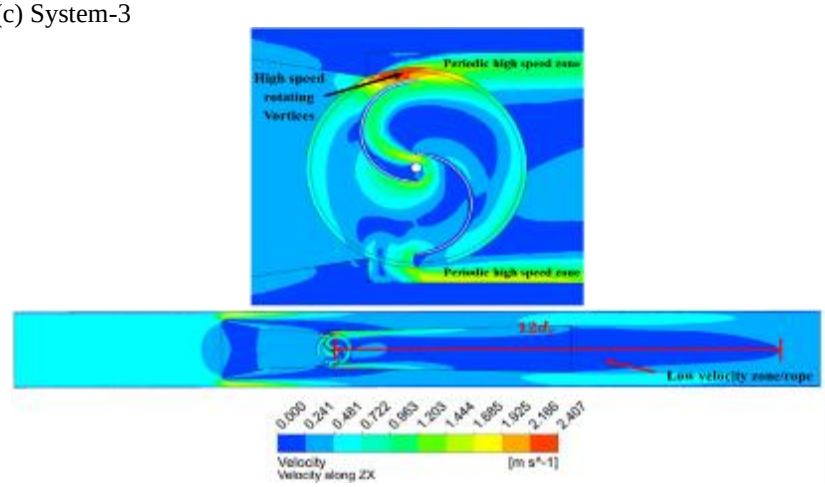

(d)System-4

Fig. 14 Velocity contour of all cases

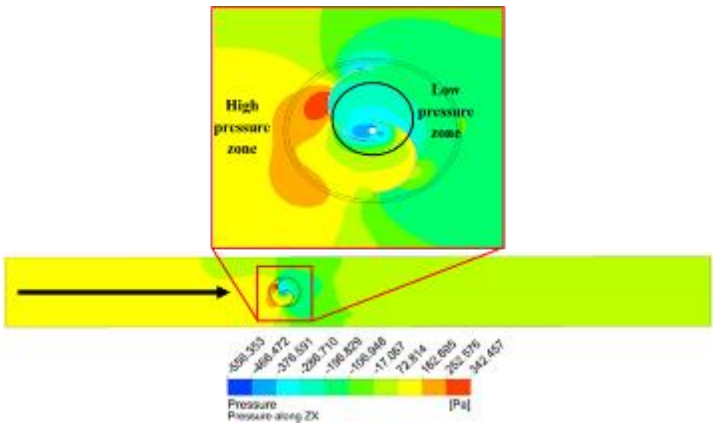

(a)System-1

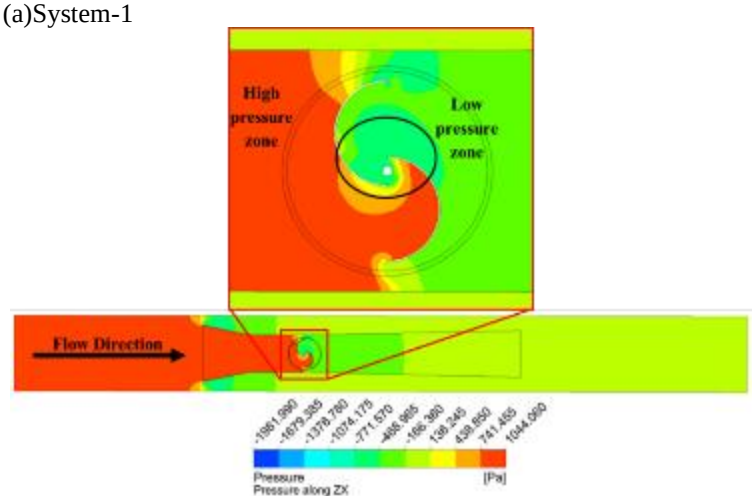

(b)System-2

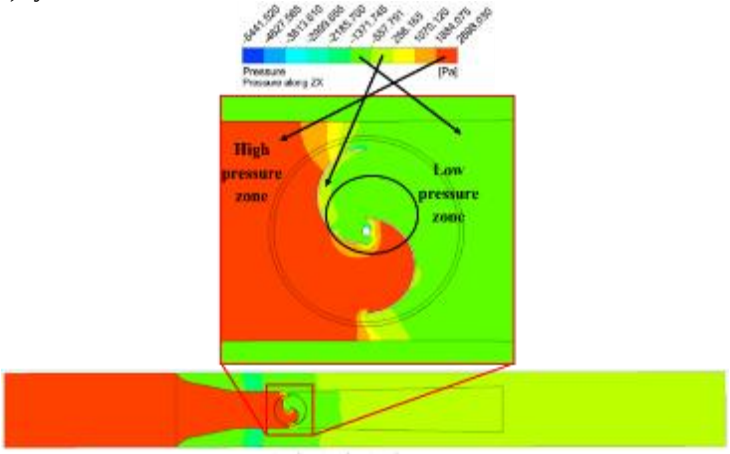

(c)System-3

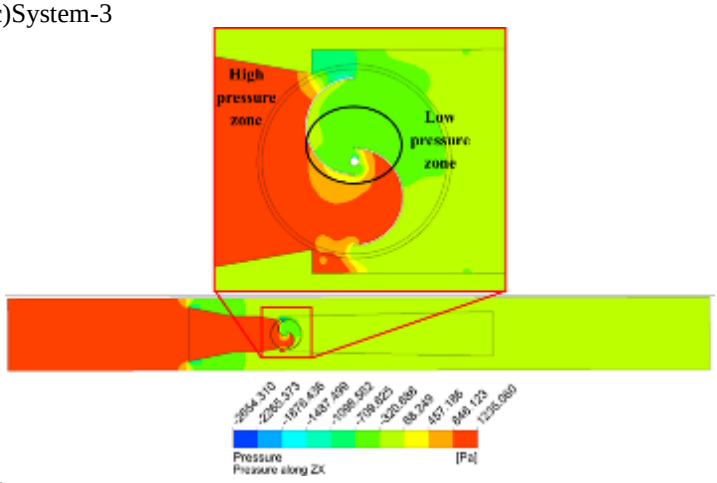

(d)System-4

Fig. 15: Pressure distribution for all systems

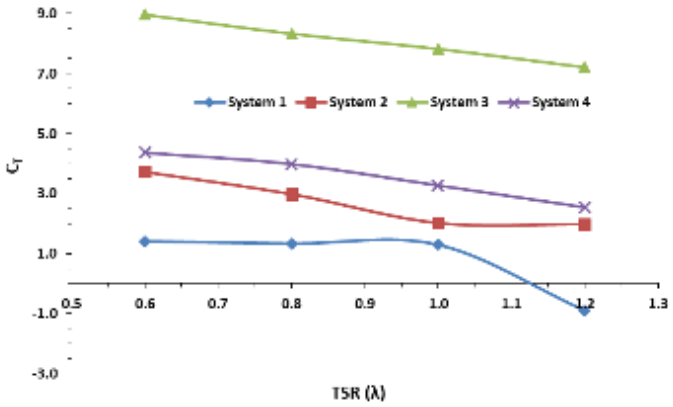

(a) Variation of torque with respect to TSR

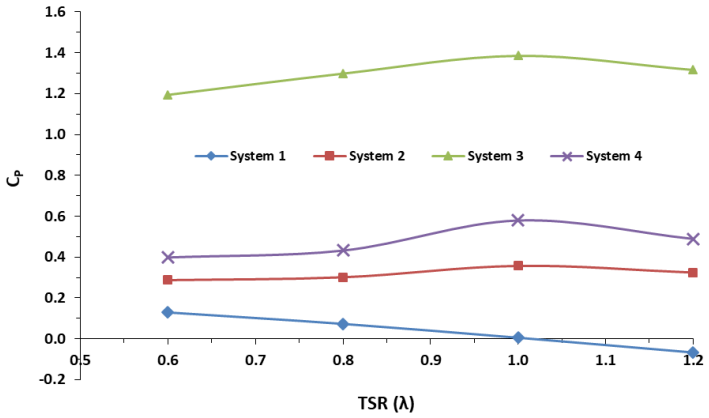

(b)Variation of power with respect to TSR

Fig. 16(a) & (b) Performance characteristic curve

advancing blade, and the pressure distribution differs between the rotor blades.

In System-1, pressure is observed to be 162 Pa at the advancing blade's concave surface and negative 376 Pa at the blade's convex side. As a result, a pressure gradient of 538 Pa is generated across the turbine blades. Similarly, pressure differences of 1815 Pa, 4883 Pa, and 1944 Pa are reported in Systems-2, 3 and 4 respectively. This pressure differential will produce drag force, and it will subsequently generate torque. Moreover, the outcomes of Systems-2, 3, and 4 are identical to the validated result of Case 1. As a consequence, System-3 with the maximum pressure differential (4883 Pa) may produce the higher drag which reflects the improvement in the performance.

5.3 Performance Characteristic of Torque (C_T) & Power (C_P)

The variation of the torque and power coefficients at various TSRs for the Savonius Hydrokinetic Turbine and its enhanced method is depicted in Fig. 16 (a). These findings indicate that the proposed arrangement of positioning the turbine within the ducted structure has an effect on the rotor torque coefficient. As the TSR or rotational speed was reduced, the coefficient of torque increased (RPM). The arrangement of System-3 increases the torque coefficient. Additionally, other two variant systems i.e., System-2 and System-4 had performed well than System -1 (solely Savonius turbine). The coefficient of performance increases with decreasing of TSR until it reaches the maximum value for each system.

Figure 16(b) illustrates the coefficient of performance corresponding to TSR. System-3 consistently outperforms the other systems across all TSR values. Additionally, the maximum coefficients of performance for Systems 2, 3, and 4 were 0.357, 1.385, and 0.579 respectively, achieved at $\lambda = 1$, compared to System-1, which reached a maximum C_P of 0.129 at $\lambda = 0.6$.

6. CONCLUSIONS

Computational analysis was conducted to assess the performance of various configurations of a Savonius turbine. The turbine was tested under site-specific conditions with an average water velocity of 0.58 m/s. Numerical investigations were performed using the commercial CFD software FLUENT. Flow visualization included consideration of factors such as pressure and velocity distributions. Additionally, the study evaluated the coefficients of torque and power. The principal findings of this investigation are summarized as follows:

- The computationally observed results are found similar with findings from the previous studies qualitatively as well as quantitatively.

- Regarding velocity contours, a wake zone was observed behind the rotor and a pressure drop occurred across the rotor from the upstream to the downstream side. This pressure difference across the rotor causes the turbine rotation resulting in extraction of power from the flowing water in the channel or canal.
- The suggested variant systems arrangement can enhance the pressure differential, allowing more flow to be sucked into the turbine resulting in all three variant systems performing better than solely Savonius turbine
- The lowest C_T & C_P was found for the solely Savonius turbine considered in the canal. The torque coefficient and power coefficient were 7.814 Nm and 1.385 respectively for the System-3 i.e., deflector section provided before the flume, and was maximum amongst all other systems. This power value can be utilized for any small isolated systems.
- The maximum C_P is obtained at λ of 1 for three suggested variant systems. However, for the System-1 i.e., solely Savonius turbine, the maximum C_P is found at λ ratio of 0.6.

The study concludes that deploying a standalone Savonius turbine directly in canals or water flow streams may not be optimal. Instead, employing a variant system with a flume and a deflector section at the inlet proves more effective. Such systems can generate sufficient power density for small isolated systems. Further verification of these findings is required through experimental methods. Additionally, investigating the performance impact while considering the blockage ratio parameter using both numerical and experimental approaches is recommended.

ACKNOWLEDGEMENTS

Authors wish to acknowledge the financial support by the Gujarat Council on Science and Technology (GUJCOST), Department of science and technology, Government of Gujarat under the STI Policy, grant vide their letter no. GUJCOST/STI/2020-21/2268 dated March 25, 2021. Also, the technical support provided by the UKAI left bank canal authority is highly appreciated.

CONFLICT OF INTEREST

The authors declare that they have no known competing financial interests or personal relationships that could have appeared to influence the work reported in this paper.

AUTHORS CONTRIBUTION

Pankaj P. Gohil: Writing-original draft, conceptualize, Experimentation. **Vimal K. Patel**: Reviewing & Editing. **Amit U. Meht:** Experimentation, Writing, Editing.

REFERENCES

Alizadeh, H., Jahangir, M. H., & Ghasempour, R. (2020). CFD-based improvement of Savonius type hydrokinetic turbine using optimized barrier at the low- speed flows. *Ocean Engineering*, *202*, 1-8. https://doi.org/10.1016/j.oceaneng.2020.107178

Asim, T., Mishra, R., Ubbi, K., & Zala, K. (2013). Computational fluid dynamics based optimal design of vertical axis marine current turbines. *Procedia CIRP*, *11*, 323–327. https://doi.org/10.1016/j.procir.2013.07.023

Castelli, M. R., Englaro, A., & Benini, E. (2011). The darrieus wind turbine: proposal for a new performance prediction model based on CFD. *Energy*, *36*(8), 4919–4934. https://doi.org/10.1016/j.energy.2011.05.036

Chen, Y., Guo, P., Zhang, D., Chai, K., Zhao, C., & Li, J. (2022). Power improvement of a cluster of three Savonius wind turbines using the variable-speed control method. *Renewable Energy*, *193*, 832-842. https://doi.org/10.1016/j.renene.2022.05.062.

Driss, Z., Jemni, M. A., Chelly, A., & Abid, M. S. (2013). Computational study of a vertical axis water turbine placed in a hydrodynamic test bench. *International Journal of Mechanics and Applications*, *3*(4), 98–104. https://doi.org/10.5923/j.mechanics.20130304.06

Elbatran, A. H., Ahmed, Y. M., & Shehata, A. S. (2017). Performance study ofducted nozzle Savonius water turbine, comparison with conventional Savonius turbine. *Energy*, *134*, 566-584. https://doi.org/10.1016/j.energy.2017.06.041

Golecha, K., Eldho, T. I., & Prabhu, S. V. (2011). Influence of the deflector plate on the performance of modified Savonius water turbine. *Applied Energy*, *88*(9), 3207–3217. https://doi.org/10.1016/j.apenergy.2011.03.025

Golecha, K., Eldho, T. I., & Prabhu, S. V. (2012). Performance study of modified Savonius water turbine with two deflector plates. *International Journal of Rotating Machinery*, 1-12. https://doi.org/10.1155/2012/679247

IEC 60041/IS 41. 1991. Field acceptance tests to determine the hydraulic performance of hydraulic turbines storage pumps and pump turbines. *Bureau of Indian standards*, New Delhi. https://archive.org/details/gov.in.is.iec.41.1991

Johnson, J. B., & Pride, D. J. (2010). River, tidal, and ocean current hydrokinetic energy technologies: status and future opportunities in Alaska. *Alaska Centre for Energy and Power*. Chrome-extension://efaidnbmnnnibpcajpcglclefindmkaj/https://tethys.pnnl.gov/sites/default/files/publications/Johnson_Pride_2010.pdf

Kerikous, E., & Thévenin, D. (2019). Optimal shape and position of a thick deflector plate in front of a

hydraulic Savonius turbine. *Energy*, *189*, 116-157. https://doi.org/10.1016/j.energy.2019.116157

Kolekar, N., & Banerjee, A. (2015). Performance characterization and placement of a marine hydrokinetic turbine in a tidal channel under boundary proximity and blockage effects. *Applied Energy*, *148*, 121-133.

Kumar, A., & Saini, R. P. (2017a). Performance analysis of a single stage modified Savonius hydrokinetic turbine having twisted blades. *Renewable Energy*, *113*, 461-478. https://doi.org/10.1016/j.renene.2017.06.020

Kumar, A., & Saini, R. P. (2017b). Performance analysis of a Savonius hydrokinetic turbinehaving twisted blades. *Renewable Energy*, *108*, 502-522. https://doi.org/10.1016/j.renene.2017.03.006

Kusakana, K., & Vermaak, H J. (2013). Hydrokinetic power generation for rural electricity supply: case of South Africa. *Renewable Energy*, *55*, 467–73. https://doi.org/10.1016/j.renene.2012.12.051

Loureiro, J. B. R., & Silva Freire, A. P. (2005). Experimental investigation of turbulent boundary layers over steep two-dimensional elevations. *Journal of Brazilian Society of Mechanical Sciences and Engineering*, 27(4), 329-344. https://doi.org/10.1590/S1678-58782005000400001

Mohamed, M. H. (2012). Performance investigation of H-rotor Darrieus turbine with new airfoil shapes. *Energy*, 47(1), 522–530. https://doi.org/10.1016/j.energy.2012.08.044

Mohamed, M. H. (2013). Impacts of solidity and hybrid system in small wind turbines performance. *Energy*, 57(1), 495–504. https://doi.org/10.1016/j.energy.2013.06.004

Mohamed, M. H., Ali, A. M., & Hafiz, A. A. (2015). CFD analysis for H-rotor Darrieus turbine as a low speed wind energy converter. *Engineering Science and Technology, an International Journal*, *18*(1), 1–13. https://doi.org/10.1016/j.jestch.2014.08.002

Mohamed, M. H., Janiga, G., Pap, E., & Thevenin, D. (2010). Optimization of savonius turbines using an obstacle shielding the returning blade. *Renewable Energy*, *35*(11), 2618–2626. https://doi.org/10.1016/j.renene.2010.04.007

Mohamed, M. H., Janiga, G., Pap, E., & Thevenin, D. (2011a). Multi-objective optimization of the airfoil shape of Wells turbine used for wave energy conversion. *Energy*, 36(1), 438-446. https://doi.org/10.1016/j.energy.2010.10.021

Mohamed, M. H., Janiga, G., Pap, E., & Thevenin, D. (2011b). Optimal blade shape of a modified Savonius turbine using an obstacle shielding the returning blade. *Energy Conversion and Management*, *52*(1), 236–42. https://doi.org/10.1016/j.enconman.2010.06.070

Mosbahi, M., Ayadi, A., Chouaibi, Y., Driss, Z., & Tucciarelli, T. (2019a). Performance study of a helical Savonius hydrokinetic turbine with a new deflector system design. *Energy Conversion and Management*, *194*, 55–74. https://doi.org/10.1016/j.enconman.2019.04.080

Mosbahi, M., Ayadi, A., Mabrouki, I., Driss, Z., Tucciarelli, T., & Abid, M. S. (2019b). Effect of the converging pipe on the performance of a lucid spherical rotor. *Arabian Journal for Science and Engineering*, *44*(2), 1583–600. https://doi.org/10.1007/s13369-018-3625-0

Nag, A. K., & Sarkar, S. (2021). Techno-economic analysis of a micro-hydropower plant consists of hydrokinetic turbines arranged in different array formations for rural power supply. *Renewable Energy*, *179*, 475-487. https://doi.org/10.1016/j.renene.2021.07.067.

Nakajima, M., Iio, S., & Ikeda, T. (2008). Performance of Savonius rotor for environmentally friendly hydraulic turbine. *Journal of Fluid Science and Technology*, *3*(3), 420–429. https://doi.org/10.1299/jfst.3.420

Patel, V., Bhat, G., Eldho, T. I., & Prabhu, S. V. (2017). Influence of overlap ratio and aspect ratio on the performance of Savonius hydrokinetic turbine. *International Journal of Energy Research*, *41*, 829–844. https://doi.org/10.1002/er.3670

Patel, V., Eldho, T. I., & Prabhu, S. V. (2018). Theoretical study on the prediction of the hydrodynamic performance of a Savonius turbine based on stagnation pressure and impulse momentum principle. *Energy Conversion and Management*, *168*, 545-563. https://doi.org/10.1016/j.enconman.2018.04.065

Patel, V., Eldho, T. I., & Prabhu, S. V. (2019). Velocity and performance correction methodology for hydrokinetic turbines experimented with different geometry of the channel. *Renewable Energy*, *131*, 1300-1317. https://doi.org/10.1016/j.renene.2018.08.027

Ponta, F., & Dutt, G. S. (2000). An improved vertical axis water current turbine incorporating a channelling device. *Renewable Energy*, *20*, 223–241. https://doi.org/10.1016/S0960-1481(99)00065-8

Riglin, J., Schleicher, W. C., Liu, I. H., & Oztekin, A. (2015). Characterization of a micro-hydrokinetic turbine in close proximity to the free surface. *Ocean Engineering*, 110, 270–280. https://doi.org/10.1016/j.oceaneng.2015.10.026

Roy, S., & Saha, U. K. (2013). Computational study to assess the influence of overlap ratio on static torque characteristics of a vertical axis wind turbine. *Procedia Engineering*, *51*, 694–702. https://doi.org/10.1016/j.proeng.2013.01.099

Saini, G., & Saini, R. P. (2018). A Numerical analysis to study the effect of radius ratio and attachment angle on hybrid hydrokinetic turbine performance. *Energy for Sustainable Development*, *47*, 94–106. https://doi.org/10.1016/j.esd.2018.09.005

Sarma, N. K., Biswas, A., & Misra, R. D. (2014). Experimental and computational evaluation of Savonius hydrokinetic turbine for low velocity condition with comparison to Savonius wind turbine at the same input power. *Energy Conversion and Management*, *83*, 88–98. https://doi.org/10.1016/j.enconman.2014.03.070

Shashikumar, C. M., Hindasageri, V., & Madav, V. (2021a, February). *CFD investigation of unsteady three-dimensional savonius hydrokinetic turbine in irrigation channel with varying positions for hydro power application.* AIP Conference Proceedings. AIP Publishing. https://doi.org/10.1063/5.0036472.

Shashikumar, C. M., Vijaykumar, H., & Vasudeva, M. (2021b). Numerical investigation of conventional and tapered Savonius hydrokinetic turbines for low-velocity hydropower application in an irrigation channel. *Sustainable Energy Technologies and Assessment Journal*, *43*; 100871 (Online). https://doi.org/10.1016/j.seta.2020.100871.

Singh, S. V., & Kumar, P. (2022). Study of flow characteristics of a savonius turbine inside nozzle diffuser duct. *Journal of Engineering Research*. https://doi.org/10.36909/jer.15977.

Talukdar, P. K., Sardar, A., Kulkarni, V., & Saha, U. K. (2018). Parametric analysis of model Savonius hydrokinetic turbines through experimental and computational investigations. *Energy Conversion and Management*, 158, 36-49. https://doi.org/10.1016/j.enconman.2017.12.011

Thakur, N., Biswas, A., Kumar, Y., & Basumatary, M. (2019). CFD analysis of performance improvement of the Savonius water turbine by using an impinging jet duct design. *Chinese Journal of Chemical Engineering*, *27*(4), 794-801. https://doi.org/10.1016/j.cjche.2018.11.014

Wahyudi, B., Soeparman, S., Wahyudi, S., & Denny, W. (2013). A simulation study of Flow and Pressure distribution patterns in and around of Tandem Blade Rotor of Savonius (TBS) Hydrokinetic turbine model. *Journal of Clean Energy Technologies*, *1*, 286–291. https://doi.org/10.7763/JOCET.2013.V1.65

Zhang, B., Song, B., Mao, Z., & Tian, W. (2017). A novel wake energy reuse method to optimize the layout for Savonius-type vertical axis wind turbines. *Energy*, *121*, 341–355. https://doi.org/10.1016/j.energy.2017.01.004

Zhao, Z., Zheng, Y., Xu, X., Liu, W., & Hu, G. (2009). Research on the improvement of the performance of Savonius rotor based on numerical study. *International Conference on Sustainable Power Generation and Supply*, 1–6. https://doi.org/10.1109/SUPERGEN.2009.5348197

Zhou, T., & Rempfer, D. (2013). Numerical study of detailed flow field and performance of Savonius wind turbines. *Renewable Energy*, *51*, 373–381. https://doi.org/10.1016/j.renene.2012.09.046

Appendix -I:

Uncertainty study of measurement of liquid flow in open channels-Velocity area methods as per ISO 748: 19979(E):

Number of verticals: 11

Average velocity in section: 0.51m/s

Time of exposure: 2min

Method: 5 point method

Discharge (group rating): 35 m^3/s

(i) Uncertainty in width (X'_b)

The uncertainty in the measurement of the width should be not greater than 1%. The width of the canal is 18.5 mt.

From Table E.1: $X'_b = \pm 0.3\%$

(ii) Uncertainty in depth (X'_d)

For depths up to 0,300 m the uncertainty should not exceed ±3%, and for depth over 0,300 m the uncertainty should not exceed ±1%. The depth of the canal is 4 mt.

From Table E.2: $X'_d = \pm 0.7\%$

(iii) Method of uncertainty in time of exposure (X'_e)

The values are given as uncertainties at the 95% level. We measure the velocity at point hold the instrument of 2 min.

From Table E.3: $X'_e = \pm 6\%$

(iv) Method of uncertainty in the vertical (X'_p)

We used 5 points method.

From Table E.4: $X'_p = \pm 5\%$

(v) Method of uncertainty in rotating-element current – meter rating (X'_c)

The average velocity found to be 0.51 m/s.

From Table E.5: $X'_c = \pm 2\%$

(vi) Method of uncertainty for numbers of verticals (X'_m)

Percentage uncertainty in the measurement of mean velocity against the number of verticals. We considered the total 11 verticals.

From Table E.5: $X'_m = \pm 8.4\%$

Percentage systematic uncertainties are as follows. These values considered based the accuracy level of instrument,

$X''_b = \pm 0.5\ \%$

$X''_d = \pm 0.5\ \%$

$X''_c = \pm 0.5\ \%$

Then.

Method of calculating the Uncertainty by overall random uncertainty (X'_Q)

$$X'_Q = \pm \sqrt{\left[X_m^2 + \frac{1}{m}\left(X'^2_b + X'^2_d + X'^2_e + X'^2_p + X'^2_c\right)\right]}$$

$$X'_Q = \pm\sqrt{\left[8.4^2 + \frac{(0.3 + 0.7 + 6^2 + 5^2 + 2^2)}{15}\right]}$$

$X'_Q = \pm\sqrt{70.56 + 4.4}$

$X'_Q = 8.667$

Method of calculating the Uncertainty by overall systematic uncertainty (X''_Q)

The above equation are satisfactory for estimating the precision of the measurement but do not take account of the possibility of systematic uncertainties systematic uncertainties which behaves as random uncertainties shall be estimated separately and may be combined as

$$X''_Q = \sqrt{X''^2_b + X''^2_d + X''^2_c}$$

$X''_Q = \sqrt{(0.5^2 + 0.5^2 + 0.5^2}$ = 0.87 %

Method of combining uncertainty (X_Q):

$X_Q = \pm\sqrt{8.667^2 + 0.87^2} = 8.705\%$

Remarks:

The discharge = 35 m^3/s

The random uncertainty = ± 8.667 (95% confidence level)

Systematic uncertainty = ± 0.87 %

APPENDIX -II

Detail of the Savonius turbine:

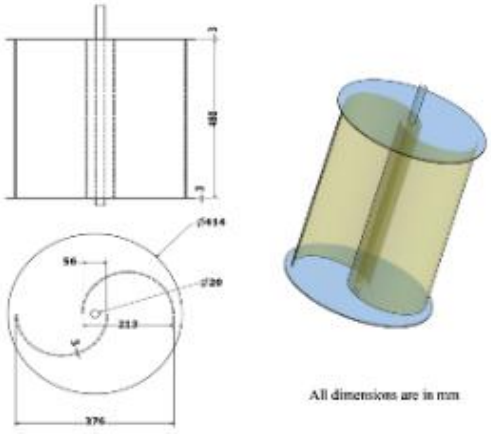

Parameter	Value
Rotor diameter (D)	376 mm
Rotor height (H)	480 mm
Aspect ratio (H/D)	1.28
End plate diameter (De)	414 mm
Blade diameter (d)	213 mm
Blade thickness (tb)	3 mm
No. of blades (Nb)	2
Blade profile	Semi-circle
Overlap ratio (e/d)	0.26
Overlap distance (e)	56 mm
Shaft diameter (Ds)	20 mm

APPENDIX-III

Mathematical Formulation:

The flow environment surrounding the Savonius turbine is complicated owing to flow separation and wake production. This sort of sophisticated unsteady flow physics is challenging to represent using typical technologies. At the moment, the most powerful instrument for this is fluid dynamics computation. Turbulence is a critical aspect in understanding the accurate modelling of the fluid domain around a Savonius turbine. There are several turbulence models available for modifying flow depending on rotor configuration and Reynolds number. The Spalart-Allmaras (SA) model, standard k-ε turbulence model, Realizable k-ε turbulence model, RNG k-ε turbulence model, Shear stress transport (SST) k-ω model, and standard k-ω model can be utilised for turbine-related simulations. The SST k-ω model (Ponta & Dutt, 2000; Asim et al., 2013; Riglin et al., 2015), the standard k-ε turbulence model (Driss et al., 2013; Roy & Saha, 2013; Wahyudi et al., 2013), the realizable k-ε turbulence model (Mohamed et al., 2010; Castelli et al., 2011; Mohamed et al., 2011a, b; Mohamed, 2012, 2013; Zhou & Rempfer, 2013; Mohamed et al., 2015), and the RNG k-ε turbulence model (Roy & Saha, 2013) have all been examined, thus far. Previous research (Sarma, et al., 2014; Kumar & Saini, 2017a, b; Mosbahi, et al., 2019a,b; Saini & Saini, 2018) revealed that the realisable k-ε turbulence model, the simplest complete turbulence model in which the solution of two separate transport equations allows the turbulent velocity and length scales to be determined independently, is best suited for hydrokinetic turbine computation simulation. As a consequence, in this work, the realisable k-ε was employed as a turbulence model to analyse the rotational behaviour of turbine blades.

The fundamental assumption of the k-ε model is that the flow is entirely turbulent, neglecting the influence of molecular viscosity and thereby limiting its applicability to fully turbulent flows. However, a newer variant known as the realizable k-ε model deviates from the standard k-ε model in two significant aspects: (i) A new formulation for turbulent viscosity is included in the realizable k-ε model and (ii) A new transport equation for ε has been derived from an exact equation for the transport of the mean-square vorticity fluctuation. Additionally, in flows including rotation, boundary layers under significant unfavourable pressure gradients, recirculation and separation the Realizable k-ε model outperforms other models. In the Realizable k-ε model, the modelled transport equations for k and ε may be stated as follows:

$$\frac{\partial}{\partial t}(\rho k) + \frac{\partial}{\partial x_j}(\rho k u_j) = \frac{\partial}{\partial x_j}\left[\left(\mu + \frac{\mu_t}{\sigma_k}\right)\frac{\partial k}{\partial x_j}\right] + G_k + G_b - \rho\varepsilon - Y_M + S_k$$

$$\frac{\partial}{\partial t}(\rho \varepsilon) + \frac{\partial}{\partial x_j}(\rho \varepsilon u_j) = \frac{\partial}{\partial x_j}\left[\left(\mu + \frac{\mu_t}{\sigma_k}\right)\frac{\partial \varepsilon}{\partial x_j}\right] + \rho C_1 S_\varepsilon - \rho C_2 \frac{\varepsilon^2}{k + \sqrt{v\varepsilon}} + C_{1\varepsilon}\frac{\varepsilon}{k} C_{3\varepsilon} G_b + S_\varepsilon$$

Where:

$$C_1 = max[\,0.43, \frac{\eta}{\eta + 5}]$$

$$\boldsymbol{\eta = S\frac{k}{\varepsilon}}$$

$$S = \sqrt{2S_{ij}S_{ij}}$$

G_k = Generation of turbulent kinetic energy due to the mean velocity gradients

G_b = Generation of turbulent kinetic energy due to buoyancy

Y_M = Contribution of the fluctuating dilatation in compressible turbulence to the overall dissipation rate

C_2 and $C_{1\varepsilon}$= Constants

σ_k and σ_ε= turbulent Prandtl numbers for k and ε